



HAL
open science

Structure-from-motion, multi-view stereo photogrammetry applied to line-scan sediment core images

Kevin Jacq, Estelle Ployon, William Rapuc, Claire Blanchet, Cécile Pignol,
Didier Coquin, Bernard Fanget

► To cite this version:

Kevin Jacq, Estelle Ployon, William Rapuc, Claire Blanchet, Cécile Pignol, et al.. Structure-from-motion, multi-view stereo photogrammetry applied to line-scan sediment core images. *Journal of Paleolimnology*, 2021, 66 (3), pp.249-260. 10.1007/s10933-021-00204-x . hal-03257581

HAL Id: hal-03257581

<https://sde.hal.science/hal-03257581v1>

Submitted on 5 Sep 2021

HAL is a multi-disciplinary open access archive for the deposit and dissemination of scientific research documents, whether they are published or not. The documents may come from teaching and research institutions in France or abroad, or from public or private research centers.

L'archive ouverte pluridisciplinaire **HAL**, est destinée au dépôt et à la diffusion de documents scientifiques de niveau recherche, publiés ou non, émanant des établissements d'enseignement et de recherche français ou étrangers, des laboratoires publics ou privés.

Structure-from-Motion, Multi-View Stereo photogrammetry applied to line-scan sediment core images

Kévin Jacq^{1,2}, Estelle Ployon³, William Rapuc¹, Claire Blanchet¹, Cécile Pignol¹, Didier Coquin², Bernard Fanget¹

1 Univ. Grenoble Alpes, Univ. Savoie Mont Blanc, CNRS, EDYTEM, 73000 Chambéry, France

2 Laboratoire d'Informatique, Systèmes, Traitement de l'Information et de la Connaissance (LISTIC),
Université Savoie Mont-Blanc, 74944 Annecy Le Vieux Cedex, France

3 Laboratoire PACTE, UMR5194 - CNRS, Univ. Grenoble Alpes, Science-Po, Grenoble, France

Corresponding Author:

Kévin Jacq

UMR CNRS 5204 Environnements, Dynamiques et Territoires de la Montagne (EDYTEM)

Université Savoie Mont Blanc, Campus scientifique,

73376 Le Bourget du Lac cedex, France

jacq.kevin@hotmail.fr

Keywords: Structure from motion photogrammetry, High-resolution image, Automatic image assembly, Orthorectification, Sediment cores, Agisoft Metashape

Abstract

Images of sediment cores are often acquired to preserve primary color information, before such profiles are altered by subsequent sampling and destructive analyses. In many cases, however, no post-processing of these images is undertaken to extract information, despite the fact that image processing can be used to describe and measure structures within the sample. Improvements of RGB (Red/Green/Blue) cameras and image processing algorithms now enable acquisition of high-resolution, metrically calibrated pictures called ortho-images, which have great potential. The way to obtain such ortho-images is by processing several raw images. We propose a semi-automated method that uses metrically calibrated targets to create the ortho-image, using Agisoft Photoscan software and a Python script. The method was tested on sediment cores up to 1.5 m long. It was compared to an approach without markers, one that uses only image matching. The proposed method showed better resolution and less distortion (GSD: 59 μm , RMSE: 7-18 μm). Images acquired without calibrated targets can still be used, by manually positioning points that can then be metrically calibrated. This approach is very useful for smartphone images taken in the field. There are many potential applications for such images of sediment cores, for instance as metric stratigraphic logs to facilitate description of the profile by unit, to study and measure structures (e.g. laminae, instantaneous deposits), or use of image registration or data fusion to create spatial landmarks for non-destructive sensors or destructive laboratory analyses. High-resolution metrically calibrated RGB images of sediment cores are simple to acquire and can play an important role in paleoclimate and paleoenvironmental studies.

Introduction

Paleoclimate and paleoenvironmental conditions are frequently inferred from natural archives such as lake and marine sediment cores, tree rings, corals and speleothems (PAGES2k Consortium 2017). These archives are often sampled for multiple physical, chemical and biological analyses. Prior to sampling, the archives are sometimes imaged with an RGB camera, a process that is rapid, cheap and simple, and used to preserve primary information, e.g. about color and structure. Such images are, however, rarely exploited to extract relevant environmental information, which can be accomplished using image processing techniques. Characterization of structures such as laminae or instantaneous deposits enables creation of spatial landmarks that can be matched with other analyses, but requires high-resolution images.

Structure-from-Motion, Multi-View-Stereo (SfM-MVS) photogrammetry is gaining interest in the Geosciences, as a method to model object surfaces at high resolution. It enables use of 2D images, taken at different orientations and positions, for construction of a 3D structure in color. SfM-MVS is widely used to reconstruct topography in contexts where other methods, such as LiDAR, cannot be used (Smith et al. 2015; James et al. 2019). Eltner et al. (2016) summarized articles on SfM-MVS published between 2012 and 2016, and noted an increase in numbers of papers across all disciplines, e.g. soil science, volcanology, glaciology, fluvial and coastal morphology. Objects such as bones or archaeological artifacts can also be reconstructed with SfM-MVS (Falkingham 2013; Marchal and Lygren 2017), as can trees, for forest monitoring and management (Piermattei et al. 2019). SfM-MVS has proven itself in the laboratory, with results similar to a scanner. Airborne SfM-MVS has been shown to provide better reconstruction quality than other methods, at much lower cost (Cawood et al. 2017; Bilmes et al. 2019).

Some environmental samples possess periodic structures associated with natural cycles (seasonal, annual, or multi-annual) or instantaneous events (e.g. floods, avalanches, volcanic eruptions). Several studies have attempted to identify and count such periodic structures using imaging techniques (Meyer et al. 2006; Weber et al. 2010; Ndiaye et al. 2012; Vannière et al. 2013; Ebert and Trauth 2015; Zolitschka et al. 2015), but have run into problems because the resolution of images is insufficient, i.e. they have too few pixels to distinguish structures. Structural and spatial variations along the lengths of sediment cores are reflected in laminae discontinuities, changing shapes, and heterogeneous colors. Sample texture can sometimes be determined by detecting particle edges under a microscope (Francus et al. 2002; Lewis et al. 2010) or by using a standard photographic image (Rubin 2004; Baptista et al. 2012). The main challenge for detecting structures is image resolution.

High-resolution images have application for fusion of data related to: (1) laboratory destructive analyses and (2) non-destructive sensors. Multiple images of a sample, collected at various dates, enable estimation of sample deformation, which can be corrected with image registration (Liu et al. 2011). Creating a time-independent spatial landmark permits comparison of multiple analyses (e.g. organic matter, mineralogy, spectroscopy), or fusion of such measures to infer paleoclimate or paleoenvironment conditions more accurately.

Studies were conducted in remote sensing to improve the spatial resolution (nD with $n < 100$) of multispectral sensors, using a high-resolution 2D image. This approach is called pansharpening. It essentially merges high-resolution panchromatic and low-resolution multispectral imagery to create a single, high-resolution color image (Alparone et al. 2007; Vivone et al. 2015). Recently, in remote sensing that utilizes hyperspectral sensors (nD with $n > 100$), pansharpening methods were improved to fuse panchromatic, multi- and hyper-spectral images, in a new method called hypersharpening (Selva et al. 2014; Yokoya et al. 2017). Based on these studies, it was shown that an environmental

sample's high-resolution image can be the basis for fusion with other laboratory sensors (hyperspectral images from several spectroscopic ranges, CT-scans).

Recent improvements of standard RGB cameras have enabled acquisition of high-resolution core images at low cost, with micrometric pixel size for small core samples. For longer core samples, the straightforward way to acquire images is to raise the camera, but this reduces resolution. Alternatively, one can take multiple close-up images along the length of a core and then assemble them. This method, however, requires several steps that can be time-consuming and create measurement uncertainties. We propose a semi-automatized method to create a high-resolution orthorectified image, sometimes called an orthomosaic image or ortho-image, from several close-up images. This method is based on the recent development of Structure-from-Motion Multi-View-Stereo (SfM-MVS) methods and uses metrically calibrated markers to estimate and correct distortions. This simple, low-cost method was used in this study to generate sediment core images. Acquired images were then processed for sediment strata determinations and fusion of data. We discuss how the approach can be employed in the field, where images are obtained with a smartphone.

Materials and methods

The ortho-image is a metrically calibrated image, corrected for three main deformations (Chandler et al. 2005). The first results from the sensor causing optical distortion, the second is caused by the sensor position around the sample for each image, and the third by characteristics of “relief” on the sample surface (e.g. holes, fissures). The proposed method estimates these deformations and corrects them to create the ortho-image (Fig. 1a).

Image acquisition

Core images were acquired with a 2.5-m-long, manually moved tray and a Nikon D80, 10.2-megapixel camera with an AF Nikkor 35-mm lens (Fig. 2). The camera was fixed at a height of 32 cm above the core sample, providing a nadir viewing angle and enabling imaging of its entire width. Under these conditions, the depth of field was 3 cm. Each image spans a sediment length of 16 cm, with a ground sampling distance (GSD) of 50 μm . The tray was moved ~ 4 cm between photographs, to achieve 75% overlap recovery, such that each section is present in four images. Camera acquisition parameters were the same for all the images. Two halogen bulbs (GE Polylux XL, F18W/860) were used to illuminate the sample and all other light sources were eliminated. The lights were fixed at a height of 20 cm and calibrated to have maximum light in the center and the same light dispersion at the core's two ends. Light calibration enables recording of sample colors and is necessary for high-resolution image creation. Rulers were placed on both sides along the length of the core to estimate the positions of sediment structures.

Reference markers

Coded targets are printed markers from the software, which are placed on the rulers (Fig. 2c). Each is different (Fig. 2d) and is used as a ground control point (GCP). They are metrically calibrated by georeferencing their positions on the rulers. We assumed that the rulers and sediment cores were horizontal, to create a plane coordinate system ($z = 0$), which was used as a projection plane to create the ortho-image. By using different markers along the bench, the software can automatically detect them, thereby avoiding confusion and enabling automatic processing of the images. A Python script was then developed to find the GCP coordinates in an Excel sheet.

Coded targets must be printed on material that remains clean and is not damaged by exposure to sediment and water. They must not reflect excessive light because that will confound the algorithm. For these reasons, we selected an adhesive matte paper. Targets must also be of a size

comparable to the sample. The image should capture the entire marker, especially the central black circle. Markers we used had a diameter of 1 cm. Agisoft Metashape tutorials recommend that the radius of the central black circle should be ≤ 30 pixels. These targets need to be square cut, keeping in mind that the targets are black circles on a white background. They must be placed flat, with at least three markers per raw image, i.e. 10 cm apart on our bench. Reproducible conditions during image acquisition enable semi-automatized image registration.

Automatic assembly and orthorectification

Images are processed according to the four steps below, using Agisoft Photoscan, (recently renamed Metashape) software (Agisoft LLC 2018) and Python scripts, a procedure that can be accomplished in < 15 minutes. This software is simple to use and has many automatic functionalities that do not require advanced photogrammetry skills. It can be used for different objects, which vary in size and number, and has scripts to automate processing. The four steps of the proposed method (Fig. 3) are described below.

Image correction

Camera images possess optical and geometrical aberrations and deformations, which result in pixels that are not truly square. This is caused by lens distortion. Camera calibration is done to estimate geometric corrections that must be made to obtain the true shape of the sample. Such distortions are estimated using Brown's distortion model (Brown 1966). To accomplish the correction, a chessboard was imaged from different angles, and Agisoft Lens software was used at all corners of the squares to estimate radial and tangential distortions (Agisoft LCC 2011). Under our laboratory conditions, the images also presented barrel distortion. The camera calibration was then fixed in the

software and applied to all subsequent images. White balance was established to obtain colors and calibrate them for the multi-view stereo image matching step.

Registration and assembly

First, thousands of features were automatically selected within each image and the GCPs were detected. Then, image and feature matching were undertaken with the structure-from-motion (SfM) process. It enables estimation of the features, GCPs, and camera positions for each image, and creation of a "sparse" 3D tie-point cloud. The GCPs create spatial landmarks to georeference the model and optimize the optical distortion and sensor position estimates. Finally, a dense cloud was estimated with multi-view-stereo (MVS) matching of the pixels between images acquired at the different camera positions.

In the case of images that do not use GCPs, a curved shape, i.e. the well-known "dome or arc effect" can appear (James and Robson 2014), caused by misestimation of pixel positions in the x, y, and z dimensions (background axis of Fig. 4.a), and typical of linear image acquisition (Faure et al. 2014). Initial qualitative evaluation consists of visually verifying the absence of these effects. Marker position errors (as root mean square errors, RMSE) in the three dimensions (x,y,z) were also estimated using the distance between marker coordinates on several images (Verma and Bourke 2019). It is recommended that the model's accuracy be evaluated with checkpoints that were not used for model estimation (Sanz-Ablanedo et al. 2018). If the image alignment and dense cloud quality are not sufficient, some manual optimizations are required, e.g. image corrections and added manual reference points, calibrated or not.

Mesh and orthorectification

Micro-relief was modeled to obtain a digital surface model. The algorithm uses the dense cloud points to generate a closed surface with triangle surfaces called mesh. These enables modeling of sample micro-relief, like grains, holes, agglomerates and bumps. Finally, the orthorectified image was estimated from the colorized mesh projection in a 2D space to correct the image from perspective and projective distortions. Thus, an ortho-image is a mosaic of orthorectified original images, and the essential step in its creation is white balance to detect relevant color variations.

Properties and validation of the created ortho-image

The proposed method enables creation of an orthomosaic image that is 9 cm wide and 150 cm long, with a GSD of 59 μm for our example. If a single image were made for the same sample, the GSD would be 590 μm . Two main properties need to be assessed to validate the model, error of the measurements and radiometric quality. The first corresponds to pixel adjustment succession. In an unsuitable case, such as a false camera position estimate in surface model reconstruction, shears can appear in the sample structures. As noted earlier, Photoscan estimates the reconstructed RMSE of the marker positions, which are usually \leq millimeters. We recommend use of additional checkpoints whose positions are known, in areas without markers, or use of objects of known dimensions to validate the RMSE (Sanz-Ablanedo et al. 2018). For our example, the control points RMSE is 17.43 μm and that of the check points is 15.26 μm . Radiometric quality must be checked to see if color throughout the image is consistent or if color differences and aberrations can be seen between successive images. Verification in areas where the color is known, such as for markers, rulers, or reference objects, enables validation of this criterion. It is also possible to place spatial resolution and radiometric reference targets at the sample's extremities to validate these two properties (Honkavaara et al. 2009).

Discussion

Using this method with manual targets and other types of image acquisition

This method can also be applied to images acquired by other means, for example those taken with a smartphone. Generally, in such cases, the metrically calibrated markers are not available, but rulers are used to measure the sample. The user must manually place control points for all raw images and estimate their depths using the rulers. This process will take more time than with georeferenced markers, and is user-dependent. Nevertheless, the method follows the same steps presented in Fig. 1b, using tie points and dense cloud assembly, followed by application of the mesh to create the ortho-image. Image acquisition parameters in the field, however, cannot be entirely controlled, as in the laboratory, with respect to illumination, camera height, focus, tray position, etc., so biases can be introduced into the resulting ortho-images (precision, resolution, quality, spatial and color aberrations). The camera calibration step is not performed in the field, but the software performs estimates to correct some geometric aberrations. Spatial aberrations can be reduced with images taken at multiple distances (i.e. closer or farther) and multiple angles, but this requires that more images be processed manually, with control points to avoid “dome or arc effects.” In such cases, the proposed method will be less automatized. Under non-laboratory conditions, it is sometimes necessary to make radiometric corrections in the ortho-image estimation step, to achieve consistent color along the ortho-image and correct color aberrations. It is also necessary to define precisely the selected marker positions manually or have rulers with coded markers. For this example, the RMSE is similar to those of laboratory, here the control points RMSE is 7.17 μm and that of the check points is 9.22 μm .

When an ortho-image can be estimated, it has been corrected for spatial deformations and reveals surface variations that were not visible in a single image, a consequence of the lack of perspective. This is seen in a comparison of the orange boxes in Figs. 5a and 5d. In the raw image, the surface seems to be smooth, but in the assembled one, some relief is evident. Correction for reflection, as seen in a comparison between the red boxes of Figs. 5b and 5e, illustrates another post-acquisition process. Some biases, however, will persist, for example the shadow on the left end of the core in Fig. 5c, which cannot be corrected by the proposed approach.

Applications with ortho-images

The ortho-image produced at low cost and without a specific metric camera, can be used for many applications. Metric calibration and high resolution are advantages compared to standard images. We present three potential applications for such ortho-images, from the simplest and most common to the most advanced and pioneering.

Stratigraphic log with true metrics

The ortho-image can be used in applications intended for initial core description. The following example, presented in Fig. 6, was made with the PSICAT open-source application (<https://csdco.umn.edu/resources/software/psicat>). The image was imported, after which the top and bottom (length) were defined to fix the metric, which was confirmed by the rulers. The user can then manually select the main units to be photographed, describe the stratigraphic lithology and textural information, and capture images of specific, local areas. The images can be used to describe the core and make suggestions about sampling for future analyses. Comparison of several sections from the same study site, or cross-comparison of geochemical analyses, are more efficient with well measured spatial landmarks. All structures are characterized by their true depth in the profile, thanks

to the metrically calibrated image. All such sediment measures and depth information can be saved in multiple data formats to be processed using other software.

Ortho-image for image processing

Metric calibration is useful to quantify the exact dimensions of structures (flood deposits, laminae, stratigraphic units) with image processing, if the resolution is sufficient. For example, the ortho-image with the 59 μm GSD makes it is possible to discriminate sediment structures with classification or image processing methods, and then estimate a mean length using pixel size, and study their variations through time (Meyer et al. 2006; Weber et al. 2010; Ndiaye et al. 2012; Vanni re et al. 2013; Ebert and Trauth 2015; Zolitschka et al. 2015). If particles are coarse, it may be possible to estimate particle size distributions along the length of the core (Lewis et al. 2010).

Figure 7 shows an image of a laminated sediment core segment that is 1 cm x 9 cm. RGB is a color space designed for the human eye, but some studies have shown that L*A*B* (Luminance) or HSV (Hue Saturation Value) color spaces are more appropriate for classification purposes (Bora et al. 2015; Hern andez-Hern andez et al. 2016). We selected an RGB image for this example because the two sediment structures on which we focused are different enough to be discriminated. Machine learning was used to separate two types of laminae, based on previous studies by Aymerich et al. (2016) to detect tephra layers, and Jacq et al. (2020) to discriminate instantaneous deposition events from continuous sedimentation. Creation of a classification model with Matlab (R2017a, MathWorks) was accomplished by selection of a few areas and their association to one of two classes of laminae, a step called labeling (Fig. 7b). Then, pattern recognition, with an artificial neural network, was used to develop a model that discriminates between the two classes. 70% of the labeled pixels were used in calibration and 30% in validation, the latter to test the accuracy of discrimination (percent classification accuracy). One hidden layer was used for the neural network, with two neurons. The validation accuracy of the model was 97.8%. Then, the model was used to classify each pixel in the

image (Fig. 7c). We assumed that the laminae were horizontal and parallel to create a composite image (Fig. 7d). The sum of each column was calculated, and a threshold was fixed at the half-width. If the value was greater than the half-width, the column corresponds to a light lamina, and if the value was lesser than the half-width, it corresponds to a dark lamina. It was also possible to estimate the approximate lamina thickness, in pixels and/or mm, given the resolution of the ortho-image (Fig. 7e). If the image is not calibrated, the pixels and laminae will be distorted, and the thickness will be misestimated. Advanced image processing methods, such as segmentation, can be used to study the whole width of the lamina to determine their true orientation and shape, and estimate the thickness range for each. There are two types of segmentation methods, those that take a “region approach,” which group together neighboring pixels with similar properties, and those that take a “frontier approach,” which look for transitions between regions. These methods, when applied to the classification map, can be used to discretize individual laminae.

Orthomosaic image for image registration and data fusion

RGB image acquisition was done as a first step to preserve a record of sample structure. Then destructive analyses were conducted. The position of samples is referenced at that moment and is dependent on core deformation. For instance, the core may have dried and contracted since it was first opened/extruded. Thus, sample positions (depths) must be compared with the initial orthorectified image. Image registration between the first image and others acquired after sampling, enables creation of a spatial reference, independent of time and deformation (Liu et al. 2011).

Images can be used to compare results from different analyses or fuse them to make more precise inferences about paleoclimate and paleoenvironment.

Similarly, image registration and data fusion approaches can combine the RGB image with results from other high-resolution, non-destructive sensors. For example, hyperspectral images are surface analyses that provide us with spatial and structural information, and tomography is a volume

analysis that can estimate the size and shape of particles. All these sources of information can be combined to improve our knowledge of the sample (Selva et al. 2015; Li et al. 2017; Yokoya et al. 2017). An RGB image can play an important role in this fusion process, given its high spatial resolution.

Free open function

Photoscan can use Python scripts to automatize processes. For example, to calibrate the markers, a calibration Excel sheet is opened to find core depths and associated marker codes. The Photoscan algorithm finds the markers, with their code on each image, and a comparison is made to find the depth associated with each marker on the raw images. Another script can be used to automatize all the proposed steps (tie point, dense cloud, mesh, and orthorectification). These scripts can be found at https://github.com/JacqKevin/RGB_PhotoScanOrthorectification (last accessed september 12, 2020).

This method can be carried out using other software or programming language, which may be free for many users, but may require advanced skills in photogrammetry, image processing, and programming. Among them are VisualSFM, MicMac, COLMAP and GRAPHOS (Gonzalez-Aguilera et al. 2018). According to the structure-from-motion community, each of these software packages has its own advantages/disadvantages and capabilities, but is essentially an alternative to Agisoft Photoscan/Metashape.

Marker recommendations

Markers are the most important tool used in the automatic method. If they are not printed on appropriate material, some steps can be compromised, for instance if the marker is not detected or is confused with another marker. Standard paper does not work because it is easily damaged and

gets dirty quickly. Adding polypropylene-based tape is also unsuitable. Metal stickers can be used, but are prone to being scratched. Additional ideas that remain untested include use of 3D printed plastic markers, or entire plastic rulers printed with markers. For the moment, we use adhesive matte paper. We note that the method can still be carried out if some markers are damaged. It is essential, however, to check the tie points and see if some do not work and hence compromise the model. In such cases they must be replaced.

Conclusions

Creation of high-resolution images of sediment cores is essential to preserve primary information about characteristics such as color, surface topography and grain size. Acquisition of images is the first step after core collection/extrusion, and the images must be processed further to better characterize the sample. The proposed method enables rapid creation of an ortho-image from several images, via an automated process (GSD: 59 μm , RMSE: 7-18 μm). The procedure only requires metrically calibrated markers that are recognized by Agisoft Photoscan/Metashape software. A Python script can be used to automatize all steps required to obtain the ortho-image. It may be possible to use this method with open-free tools or with a stand-alone executable program, but those may need some adaptation steps.

The orthorectified image shows great possibilities with data processing. Image processing enables classification of patterns in the sediment core, which can be used to analyze coarse (flood deposits, laminae) or fine (grain size) characteristics of the sediment. It can create a spatial landmark with other images captured on several dates, with image registration used to estimate deformations and correct them, to register all analyses conducted on the core. This new image can also be combined with information from other high-resolution, non-destructive sensors (hyperspectral image, CT-scan) to add other dimensions (volume, spectral, temporal) to stratigraphic study of the

sample. An orthomosaic-image can enable better high-resolution study of sediment cores and other environmental samples.

Acknowledgements

Cores used in this study are stored at the Environnements, Dynamiques et Territoires de la Montagne EDYTEM laboratory. We are grateful to Charline Giguët-Covex and Stéphane Guédron for the smartphone images of the Lake Huacacarpay sediment core. We also thank Pierre Sabatier, Fabien Arnaud, and Erwan Messager for the Lake Bourget (method steps) and Aiguebelette (lamination application) sediment cores. Furthermore, we thank the anonymous reviewers and Mark Brenner (Editor-in-Chief) for their helpful comments.

References

Agisoft LCC (2011) Agisoft Lens User Manual. 5

Agisoft LLC (2018) Agisoft PhotoScan User Manual. Prof. Ed. Version 1.4

Alparone L, Wald L, Chanussot J, Thomas C, Gamba P, Bruce LM (2007) Comparison of pansharpening algorithms: outcome of the 2006 GRS-S data-fusion contest. *IEEE Trans Geosci Remote Sens* 45:3012–3021. <https://doi.org/10.1109/TGRS.2007.904923>

Aymerich IF, Oliva M, Giralt S, Martín-Herrero J (2016) Detection of tephra layers in Antarctic sediment cores with hyperspectral imaging. *PLoS One* 11:1–24. <https://doi.org/10.1371/journal.pone.0146578>

Baptista P, Cunha TR, Gama C, Bernardes C (2012) A new and practical method to obtain grain size measurements in sandy shores based on digital image acquisition and processing. *Sediment Geol.* <https://doi.org/10.1016/j.sedgeo.2012.10.005>

Bilmes A, D’Elia L, Lopez L, Richiano S, Varela A, Alvarez M del P, Bucher J, Eymard I, Muravchik M, Franzese J, Ariztegui D (2019) Digital outcrop modelling using “structure-from-motion” photogrammetry: Acquisition strategies, validation and interpretations to different sedimentary environments. *J South Am Earth Sci* 96:1–16. <https://doi.org/10.1016/j.jsames.2019.102325>

Bora DJ, Gupta AK, Khan FA (2015) Comparing the performance of L*A*B* and HSV color spaces with respect to color image segmentation. *Int J Emerg Technol Adv Eng* 5:192–203

Brown D (1966) Decentering distortion of lenses - the prism effect encountered in metric cameras can be overcome through analytic calibration. *Photom Eng* 32:444–462

Cawood AJ, Bond CE, Howell JA, Butler RWH, Totake Y (2017) LiDAR, UAV or compass-clinometer? Accuracy, coverage and the effects on structural models. *J Struct Geol* 98:67–82.

<https://doi.org/10.1016/j.jsg.2017.04.004>

Chandler JH, Fryer JG, Jack A (2005) Metric capabilities of low-cost digital cameras for close range surface measurement. *Photogramm Rec* 20:12–26. <https://doi.org/10.1111/j.1477-9730.2005.00302.x>

Ebert T, Trauth MH (2015) Semi-automated detection of annual laminae (varves) in lake sediments using a fuzzy logic algorithm. *Palaeogeogr Palaeoclimatol Palaeoecol* 435:272–282. <https://doi.org/10.1016/j.palaeo.2015.05.024>

Eltner A, Kaiser A, Castillo C, Rock G, Neugirg F, Abellán A (2016) Image-based surface reconstruction in geomorphometry—merits, limits and developments. *Earth Surf Dynam* 4:359–389. <https://doi.org/10.5194/esurf-4-359-2016>

Falkingham PL (2013) Low cost 3D scanning using off-the-shelf video gaming peripherals. *J Paleontol Tech* 11:1–9

Faure P-H, Tournadre V, Beilin J, Pierrot-Deseilligny M (2014) Métrologie par photogrammétrie aéroportée légère appliquée aux digues. *Optimiser l’auscultation des ouvrages*. *XYZ* 141:47–54

Francus P, Keimig F, Besonen M (2002) An algorithm to aid varve counting and measurement from thin-sections. *J Paleolimnol* 28:283–286. <https://doi.org/10.1023/A:1021624415920>

Gonzalez-Aguilera D, López-Fernández L, Rodriguez-Gonzalvez P, Hernandez-Lopez D, Guerrero D, Remondino F, Menna F, Nocerino E, Toschi I, Ballabeni A, Gaiani M (2018) GRAPHOS – open-source software for photogrammetric applications. *Photogramm Rec* 33:11–29. <https://doi.org/10.1111/phor.12231>

Hernández-Hernández JL, García-Mateos G, González-Esquivá JM, Escarabajal-Henarejos D, Ruiz-Canales A, Molina-Martínez JM (2016) Optimal color space selection method for plant/soil segmentation in agriculture. *Comput Electron Agric* 122:124–132.

<https://doi.org/10.1016/J.COMPAG.2016.01.020>

- Honkavaara E, Arbiol R, Markelin L, Martinez L, Cramer M, Bovet S, Chandelier L, Ilves R, Klonus S, Marshal P, Schläpfer D, Tabor M, Thom C, Veje N (2009) Digital airborne photogrammetry—a new tool for quantitative remote sensing?—a state-of-the-art review on radiometric aspects of digital photogrammetric images. *Remote Sens* 1:577–605. <https://doi.org/10.3390/rs1030577>
- Jacq K, William R, Alexandre B, Didier C, Bernard F, Perrette Y, Sabatier P, Bruno W, Maxime D, Arnaud F (2020) Sedimentary structures discriminations with hyperspectral imaging on sediment cores. *EarthArXiv*. <https://doi.org/10.31223/osf.io/4ue5s>
- James MR, Chandler JH, Eltner A, Fraser C, Miller PE, Mills JP, Noble T, Robson S, Lane SN (2019) Guidelines on the use of structure-from-motion photogrammetry in geomorphic research. *Earth Surf Process Landforms* 44:2081–2084. <https://doi.org/10.1002/esp.4637>
- James MR, Robson S (2014) Mitigating systematic error in topographic models derived from UAV and ground-based image networks. *Earth Surf Process Landforms* 39:1413–1420. <https://doi.org/10.1002/esp.3609>
- Lewis T, Francus P, Bradley RS, Kanamaru K (2010) An automated system for the statistical analysis of sediment texture and structure at the micro scale
- Li S, Kang X, Fang L, Hu J, Yin H (2017) Pixel-level image fusion: A survey of the state of the art. *Inf Fusion* 33:100–112. <https://doi.org/10.1016/j.inffus.2016.05.004>
- Liu C, Yuen J, Torralba A (2011) SIFT flow: dense correspondence across scenes and its applications. *IEEE Trans Pattern Anal Mach Intell* 33:978–994. <https://doi.org/10.1109/TPAMI.2010.147>
- Marchal G, Lygren T (2017) The Microsoft Kinect: validation of a robust and low-cost 3D scanner for biological science
- Meyer MC, Faber R, Spö TI C (2006) The WinGeol Lamination Tool: new software for rapid, semi -

automated analysis of laminated climate archives. *Holocene* 16:753–761.

<https://doi.org/10.1191/0959683606hl969rr>

Ndiaye M, Davaud E, Ariztegui D, Fall M (2012) A semi automated method for laminated sediments analysis. *Int J Geosci* 3:206–210. <https://doi.org/10.4236/ijg.2012.31023>

PAGES2k Consortium (2017) A global multiproxy database for temperature reconstructions of the Common Era. *Sci Data* 4:. <https://doi.org/10.1038/sdata.2017.88>

Piermattei L, Karel W, Wang D, Wieser M, Mokroš M, Surový P, Koreň M, Tomašík J, Pfeifer N, Hollaus M (2019) Terrestrial structure from motion photogrammetry for deriving forest inventory data. *Remote Sens* 11:950. <https://doi.org/10.3390/rs11080950>

Rubin DM (2004) A simple autocorrelation algorithm for determining grain size from digital images of sediment. *J Sediment Res* 74:160–165

Sanz-Ablanedo E, Chandler JH, Rodríguez-Pérez JR, Ordóñez C (2018) Accuracy of unmanned aerial vehicle (UAV) and SfM photogrammetry survey as a function of the number and location of ground control points used. *Remote Sens* 10:1–19. <https://doi.org/10.3390/rs10101606>

Selva M, Aiazzi B, Butera F, Chiarantini L, Baronti S (2014) Hyper-sharpening of hyperspectral data: A first approach. In: 6th Workshop on Hyperspectral Image and Signal Processing: Evolution in Remote Sensing (WHISPERS). IEEE, pp 1–4

Selva M, Aiazzi B, Butera F, Chiarantini L, Baronti S (2015) Hyper-sharpening: a first approach on SIM-GA data. *IEEE J Sel Top Appl Earth Obs Remote Sens* 8:3008–3024.
<https://doi.org/10.1109/JSTARS.2015.2440092>

Smith MW, Carrivick JL, Quincey DJ (2015) Structure from motion photogrammetry in physical geography. *Prog Phys Geogr Earth Environ* 40:247–275.
<https://doi.org/10.1177/0309133315615805>

- Vanni re B, Magny M, Joannin S, Simonneau A, Wirth SB, Hamann Y, Chapron E, Gilli A, Desmet M, Anselmetti FS (2013) Orbital changes, variation in solar activity and increased anthropogenic activities: controls on the Holocene flood frequency in the Lake Ledro area, Northern Italy. *Clim Past* 9:1193–1209. <https://doi.org/10.5194/cp-9-1193-2013>
- Verma AK, Bourke MC (2019) A method based on structure-from-motion photogrammetry to generate sub-millimetre-resolution digital elevation models for investigating rock breakdown features. *Earth Surf Dyn* 7:45–66. <https://doi.org/10.5194/esurf-7-45-2019>
- Vivone G, Alparone L, Chanussot J, Dalla Mura M, Garzelli A, Licciardi GA, Restaino R, Wald L (2015) A Critical comparison among pansharpening algorithms. *IEEE Trans Geosci Remote Sens* 53:2565–2586. <https://doi.org/10.1109/TGRS.2014.2361734>
- Weber ME, Reichelt L, Kuhn G, Pfeiffer M, Korff B, Thurow J, Ricken W (2010) BMPix and PEAK tools: New methods for automated laminae recognition and counting - application to glacial varves from Antarctic marine sediment. *Geochem Geophys Geosy* 11:. <https://doi.org/10.1029/2009GC002611>
- Yokoya N, Grohnfeldt C, Chanussot J (2017) Hyperspectral and multispectral data fusion: a comparative review of the recent literature. *IEEE Geosci Remote Sens Mag* 5:29–56. <https://doi.org/10.1109/MGRS.2016.2637824>
- Zolitschka B, Francus P, Ojala AEK, Schimmelmann A (2015) Varves in lake sediments, a review. *Quat Sci Rev* 117:1–41. <https://doi.org/10.1016/j.quascirev.2015.03.019>

Figure legends

Fig. 1 Creation of an ortho-image with camera, under (a) laboratory and (b) field conditions (1) sample color and (2-3) deformation corrections. In the field, there are no camera corrections

Fig. 2 Perspectives on the sediment core image acquisition tray: (a) Side view of split core; (b) End view of split core; (c) Top (cut surface) view; (d) Examples of distinct markers. Colors in the images are coded as follows: sediment core (brown), camera (blue), illumination units (yellow), rulers (grey)

Fig. 3 The four steps of the proposed method to obtain a metrically calibrated high-resolution image (a) Tie points of the registered image, with image matching and markers, (b) A dense cloud estimates a high-resolution assembly and reconstructs 3D variations, and (a-b) Correction of inclination distortions, (c) the mesh step creates a digital surface model of the sample, with modeling of surface variations, and (d) estimated orthomosaic image, corrected from inclination and small surface reliefs

Fig. 4 Results of the low-resolution assembly (a) without markers (“arc effect”) and (b) with markers registration. The trackball shows the axis of the image (blue=x=length, green=y=width not see “green” because it is perpendicular to the page, red=z=height)

Fig. 5 Assembly of smartphone images with SFM-MVS and manual metrically calibrated markers; (a) and (b) correspond to images taken by the smartphone; (c) the ortho-image; (d) and (e) zooms of the ortho-image (orange and red boxes refer to artifacts)

Fig. 6 Log-stratigraphic metrically calibrated image of a Lake Bourget sediment core realized with PSICAT. The core was divided into two main units during which there was continuous deposition, indicated by blue and green. Event deposits are in yellow. Descriptions of the two units were made with respect to depth and sediment color

Fig. 7 Neural network pattern recognition for the determination of two laminae types, i.e. light and dark. **(a)** Raw image, **(b)** labeled areas for classification (white = light lamina, gray = dark lamina, dark = not labeled), **(c)** classification of all pixels, **(d)** reconstructed image with the predominant laminae class, on an averaged profile, **(e)** estimates of thickness of light and dark laminae

Figures

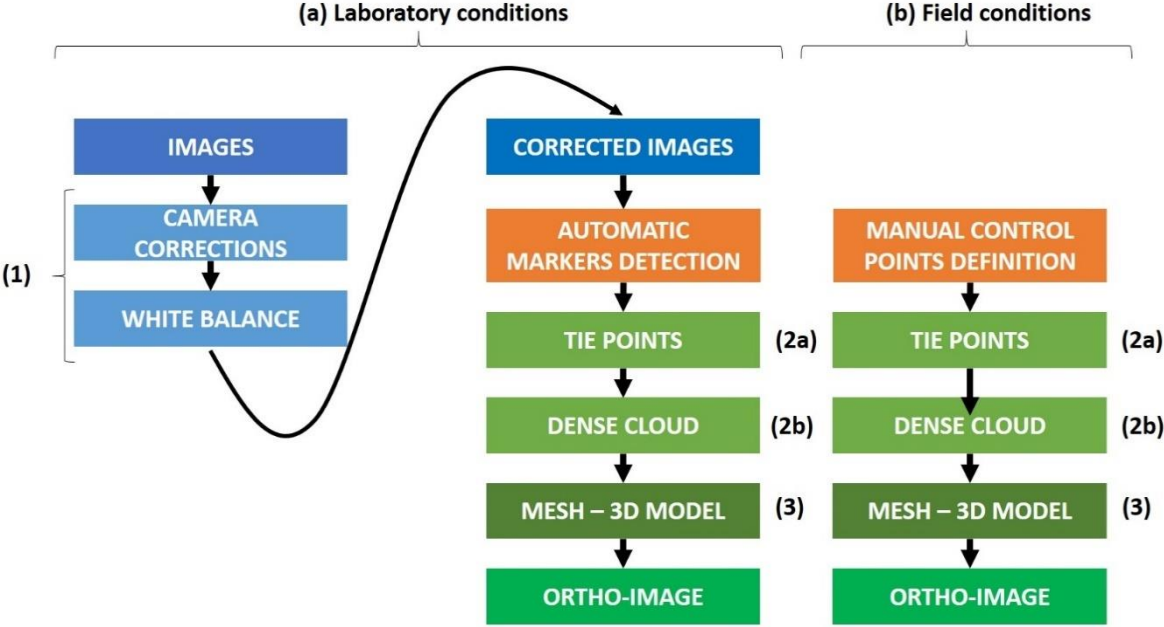


Figure 1

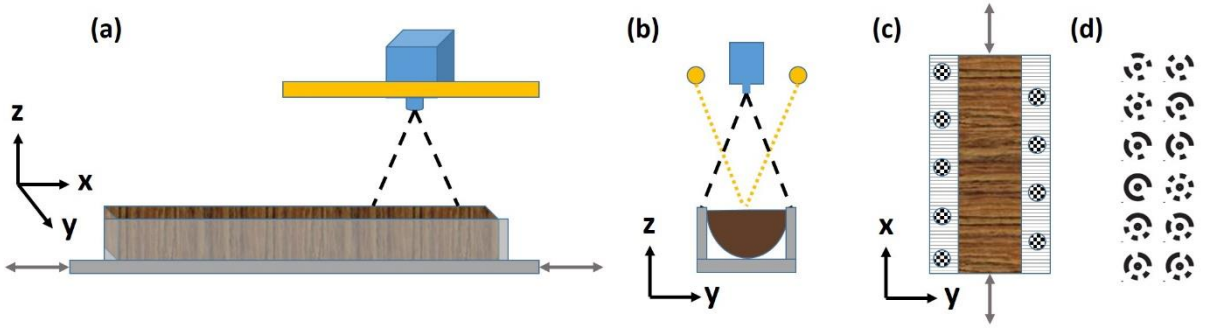


Figure 2

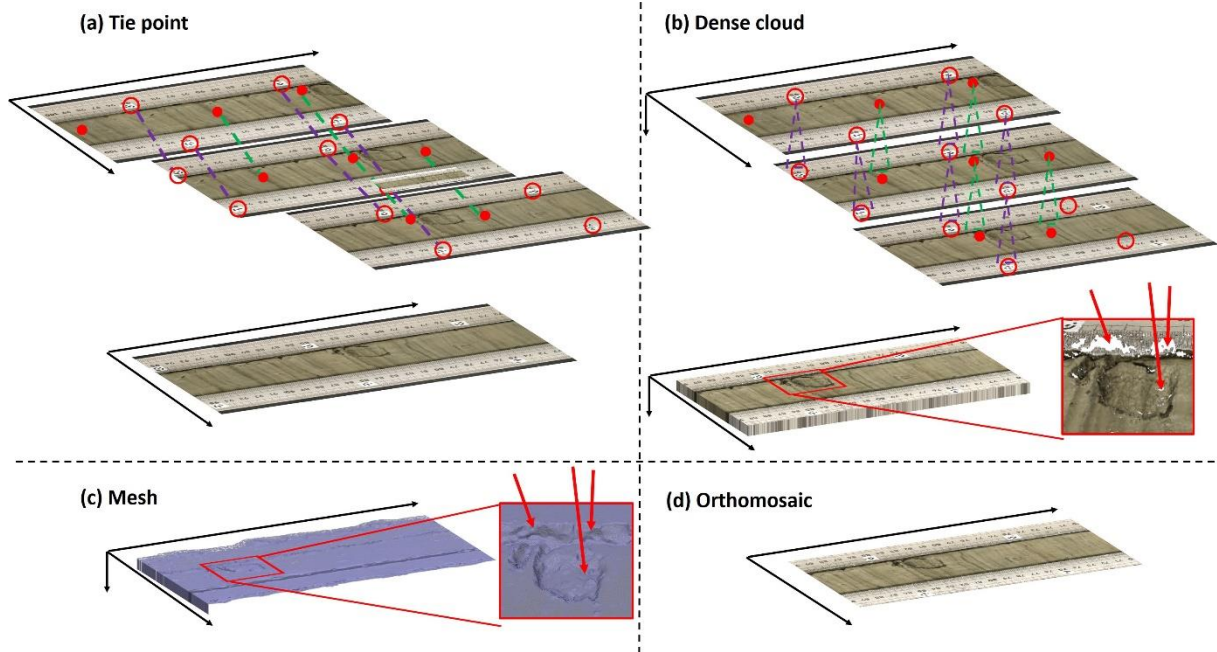


Figure 3

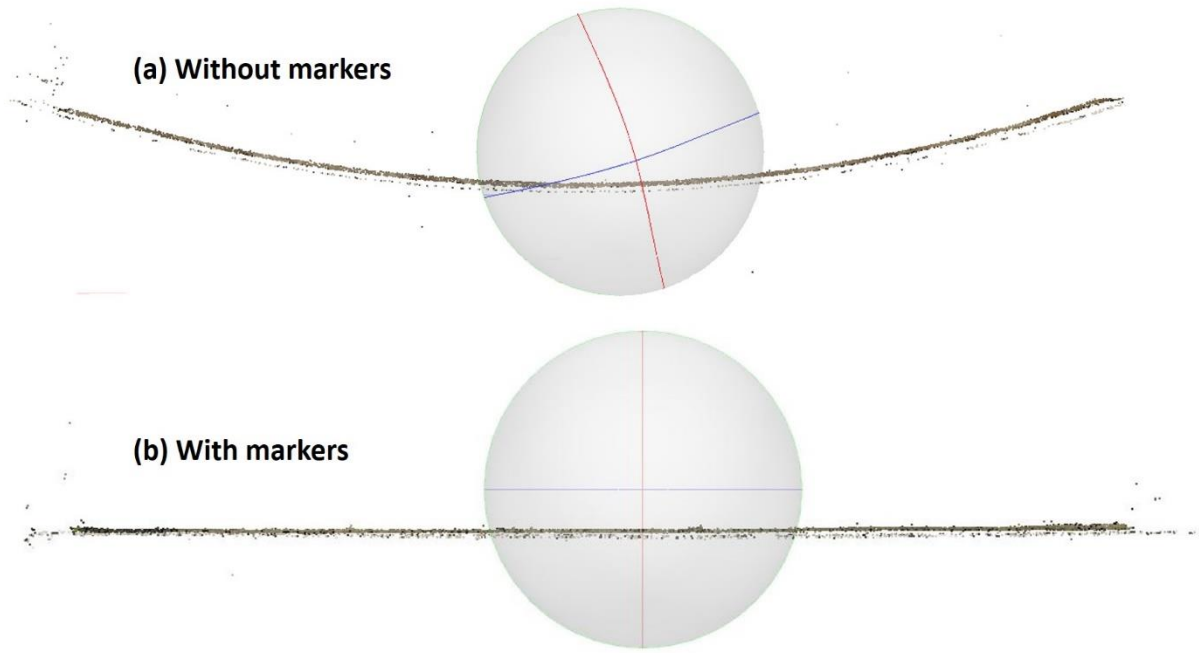


Figure 4

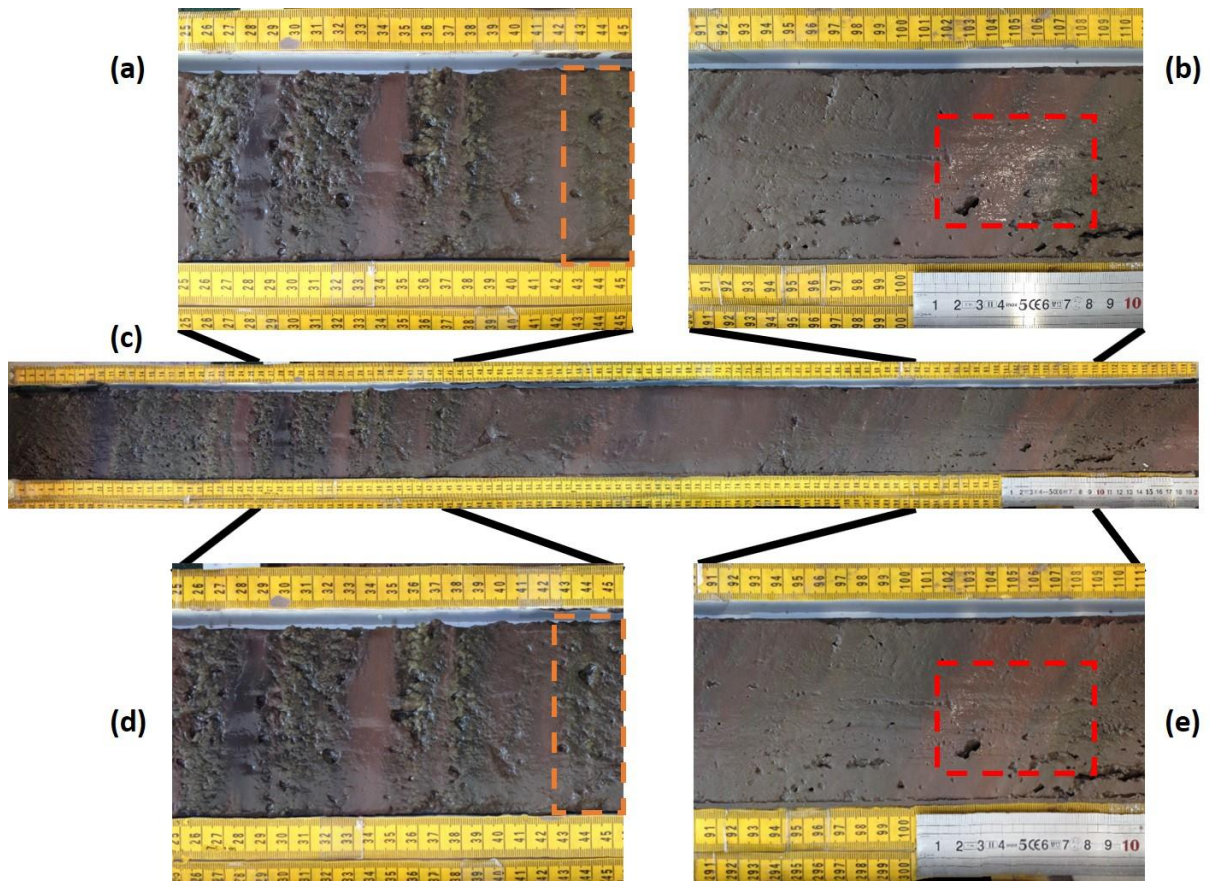


Figure 5

LDB17_P6A

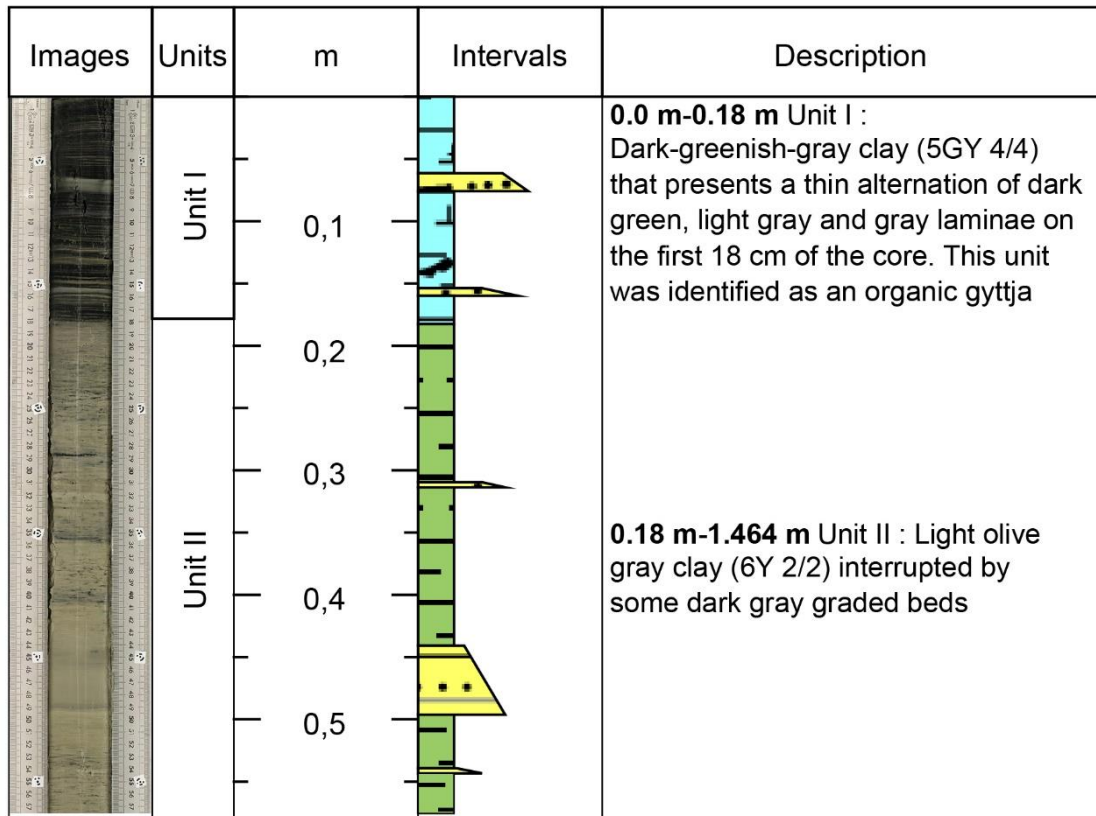


Figure 6

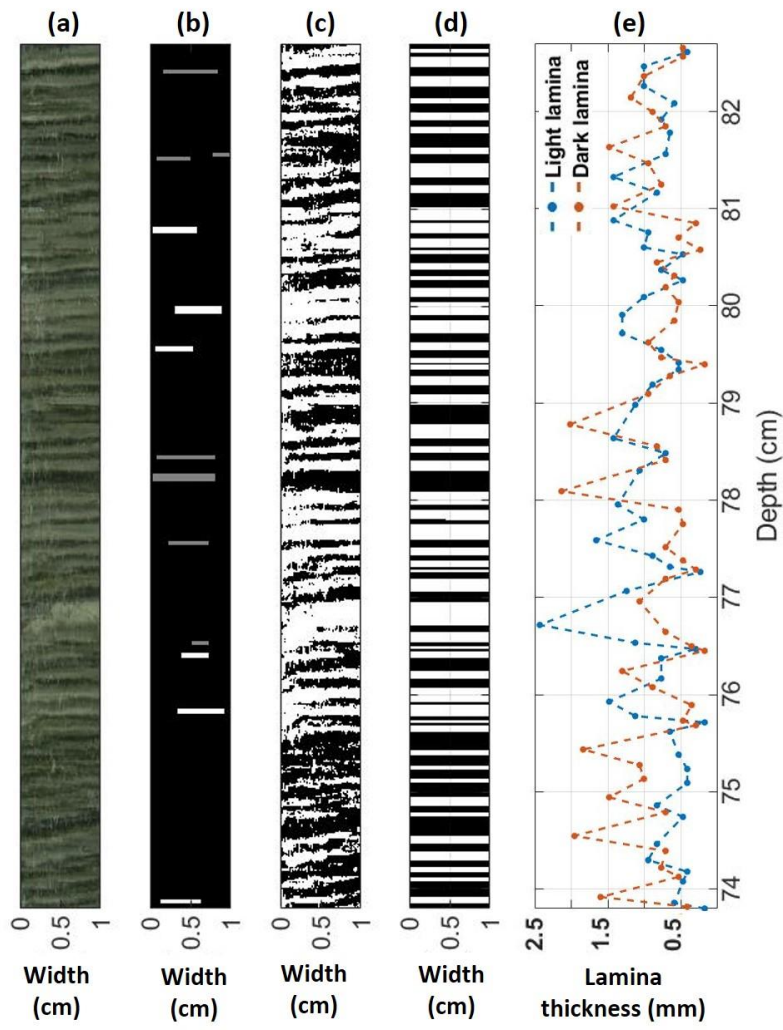


Figure 7